Macromolecules

Article

pubs.acs.org/Macromolecules

Directed Assembly of Quantum Dots Using Brush Block Copolymers for Well-Ordered Nonlinear Optical Nanocomposites

Dong-Po Song,[†] Shiva Shahin,[‡] Wanting Xie,[§] Soroush Mehravar,[‡] Xiaohui Liu,[†] Cheng Li,[†] Robert A. Norwood,[*,‡] Jae-Hwang Lee,[*,§] and James J. Watkins[*,†]

[†]Department of Polymer Science and Engineering, University of Massachusetts Amherst, 120 Governors Drive, Amherst, Massachusetts 01003, United States

[‡]College of Optical Sciences, University of Arizona, 1630 E. University Boulevard, Tucson, Arizona 85721, United States

[§]Department of Mechanical and Industrial Engineering, University of Massachusetts Amherst, 160 Governors Drive, Amherst, Massachusetts 01003, United States

Supporting Information

ABSTRACT: We report the directed assembly of quantum dots (QDs) within well-ordered photonic nanocomposites using a family of (polynorbornene-*graft*-poly(styrene))-*block*-(polynorbornene-*graft*-poly(ethylene oxide)) (PS-*b*-PEO) brush block copolymers (BBCPs). Cadmium selenide (CdSe) nanoparticles (NPs) modified with 11-mercaptoundecylhydroquinone are selectively incorporated within the PEO domains of the self-assembled BBCPs via strong hydrogen-bonding interactions between the ligands on QDs and PEO brushes of the BBCPs. Well-ordered QD arrays were readily created within a periodic lamellar polymer matrix, or one-dimensional photonic crystal, with a widely tunable lattice spacing ranging from 46.2 to up to 145 nm. The loading concentration of the QDs can be up to 30 wt % (15 vol %) while maintaining a well-ordered lamellar morphology, providing an optical gain material platform for the systematic investigation of optical properties. Strong photoluminescence and third harmonic generation from the well-ordered QD arrays were observed via multiphoton excitation using femtosecond (fs) laser light at several optical wavelengths from 700 to 1550 nm.

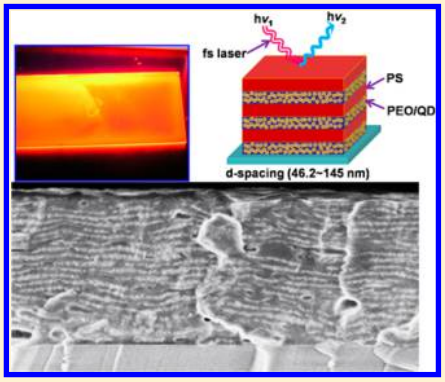

The directed self-assembly of functional nanoparticles (NPs) using block copolymers (BCPs) as the template enables precise control over the spatial distribution of NP arrays at the nanoscale level, providing a simple route to the low-cost "bottom-up" fabrication of functional hybrid materials with greatly enhanced mechanical, optical, and electric properties.[1−5] Well-ordered NP arrays are of interest for many applications including sensors, energy and memory storage devices, and nonlinear optical, plasmonic, and other optoelectronic nanodevices.[1−14]

Over the past two decades, there has been great success in the directed assembly of NPs using linear BCPs (LBCPs) with a variety of interesting structures such as periodic spherical, cylindrical, bicontinuous, and lamellar morphologies.[15−33] Favorable interactions between NPs and BCP segments are generally required to achieve the preferential sequestration of high loadings NPs within the target microdomain of a microphase-separated LBCP, effecting a balance between the enthalpic contribution due to the NP/BCP interactions and the entropic penalty arising from polymer chain stretching for NP incorporation. Generally, there are two categories of NP/BCP interactions including neutral or weak interactions,[16−24] such as van der Waals interaction, and strong interactions, such as hydrogen-bonding (H-bonding) and ionic interactions.[25−33] The loading concentration of NPs has been limited in nanocomposites with neutral NP/BCP interactions. In contrast, strong NP/BCP interactions enable the creation of nanocomposites containing much higher filling fractions of functional NPs,[26−28] which is critical for translating the attractive physical properties of NPs into promising device architectures. However, kinetically trapped morphology defects are often observed in high molecular weight BCP templates and in the highly filled nanocomposites due to the great entropic loss arising from severe perturbations of polymer chains by the large amount of NPs added.[27,32] In addition, kinetic constrain due to polymer chain entanglements in high molecular weight LBCPs limits domain sizes in well-ordered composites to a few tens of nanometers, which will limit their utility for optical applications.

The successful preparation of brush block copolymers (BBCPs) represents a major step forward in BCP-based materials and composites relative to traditional LBCPs. For instance, well-ordered lamellar morphologies can be generated in a few minutes through the self-assembly of BBCPs with high molecular weights up to 10^3 kg/mol and large domain spacing over 100 nm.[34−40] Moreover, long-range ordering has also been

Received: May 3, 2016
Revised: July 5, 2016
Published: July 13, 2016

DOI: 10.1021/acs.macromol.6b00926
Macromolecules 2016, 49, 5068−5075

achieved by rationally designed BBCPs with bulky side chains and low glass transition temperatures.[41] Recently, we reported the rapid fabrication of well-ordered nanocomposites containing high concentrations of metal NPs using amphiphilic BBCPs as the template, opening an avenue to well-ordered hybrid materials with interesting metallic photonic behaviors such as the localized surface plasmonic resonance (LSPR).[41−43] In this work, we aim to achieve the controlled assembly of another group of important functional nanomaterials, quantum dots (QDs), which have been widely used in many applications such as optical and electrical devices.[44−46] It is of great interest to study the assembly of QDs within the widely tunable BBCP domains from both fundamental and application viewpoints as this will lay the groundwork for the creation of well-ordered QD arrays for many potential applications. Light-emitting materials within a periodic lamellar polymer matrix, or one-dimensional photonic crystal, can interact with photons much more efficiently due to the anomalous optical dispersion provided by the nanostructure.[47] Besides their potential applications in cavity-less lasing and solid-state lighting, this enhancement effect can be very advantageous for multiphoton-pumped lasing exhibiting ultralow-thresholds because the two-photon absorption cross section can be enlarged due to, for example, the reduced group velocity of photons at the photonic band edges.[48−52] Compared to organic light-emitting molecules, which can readily be dispersed in a polymer matrix, QDs are generally superior over the organic molecules in resistance to various degradation processed resulting from irradiation, humidity, oxidation, and heat. Thus, the demonstration of highly loaded QDs in a periodic polymer matrix can provide an efficient and environmentally robust high gain material platform for photonics and optoelectronics.

Here, we report the simple fabrication of photonic nanocomposites containing well-ordered QD arrays via selective incorporation of the QDs into the PEO domains of self-assembled (polynorbornene-*graft*-poly(styrene))-*block*-(polynorbornene-*graft*-poly(ethylene oxide)) (abbreviated as PS-*b*-PEO) BBCPs (see Scheme 1). The domain spacing of the resulting nanocomposites is tunable within a very wide range from 46.2 to 145 nm, which is typically not available for the nanocomposites based on traditional LBCPs. The loading concentration of QDs in the nanocomposites can be as high as 30 wt % (15 vol %) without macrophase aggregation of the QDs. The obtained nanocomposites exhibit strong two-photon and multiphoton excitation emission under femtosecond (fs) laser light.

Scheme 1. Directed Assembly of QDs into Well-Ordered Lamellar Morphologies with Widely Tunable *d*-Spacings Using PS-*b*-PEO BBCPs as the Templates; the Resulting Nanocomposites Exhibit Strong Multiphoton Excitation Fluorescence under Femtosecond (fs) Laser Light

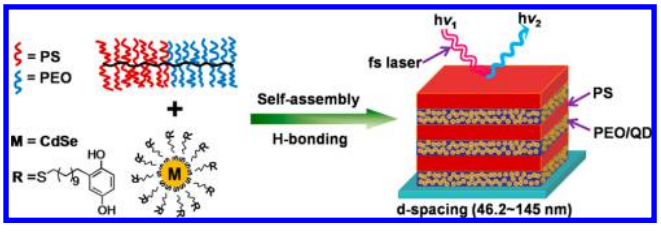

RESULTS AND DISCUSSION

The BBCPs used in this work are well-defined (polynorbornene-*graft*-poly(styrene))-*block*-(polynorbornene-*graft*-poly(ethylene oxide)) block copolymers ($(PNB-PS_{3.5K})_n$-*b*-$(PNB-PEO_{2K})_m$) synthesized by sequential ring-opening metathesis polymerization (ROMP). Detailed information regarding the synthesis and characterization of the polymers has been reported previously.[42] The molecular weight of the PS brush is 3.5 kg/mol (about 33 repeat units), while the PEO brush has a molecular weight of 2 kg/mol (about 45 repeat units). The subscripts *n* and *m* represent the degree of polymerization (DP) of each block. Molecular weight information for the polymer series has been summarized in Table 1.

Table 1. Molecular Weight Information for the (Polynorbornene-*graft*-Poly(styrene))-*block*-(Polynorbornene-*graft*-Poly(ethylene oxide)) Copolymers

BBCP	M_n[a] (kg/mol)	PDI[a]	DP[b] PSMM	DP[b] PEOMM	domain spacing[c] (nm)
A	160	1.13	26	32	43.6
B	185	1.16	30	43	53.2
C	285	1.38	49	60	79.5
D	374	1.41	63	77	95.2
E	487	1.45	86	104	106
F	995	1.28	142	248	123
G	1150	1.36	177	264	161
H	1330	1.49	190	332	185

[a]Molecular weight and polydispersity index as measured by GPC-MALLS. [b]Approximation of the size of each block as calculated using NMR and GPC results. [c]The domain spacing (*d*-spacing) as determined by SAXS data in Figure 1 or by image analysis of TEM in Figure S1 (Supporting Information).

Small-angle X-ray scattering (SAXS) was used to determine the bulk morphology and the lattice parameter of these BBCPs. Bulk samples were prepared within the inner diameter of stainless steel washers and sandwiched between Kapton films. Samples **A**−**E** were kept on a hot plate at 130 °C for 5 min, while samples **F**−**H** of higher molecular weights were annealed at 120 °C under vacuum for 24 h to achieve thermal equilibrium before SAXS measurements. The self-assembly of the BBCPs into well-ordered lamellar morphologies was observed after thermal annealing as indicated by the SAXS data in Figure 1. For example, the SAXS profile of BBCP **F** shows a sharp primary peak at a scattering vector (q) of 0.051 nm^{-1}, indicating strong phase separation of the BCP into a

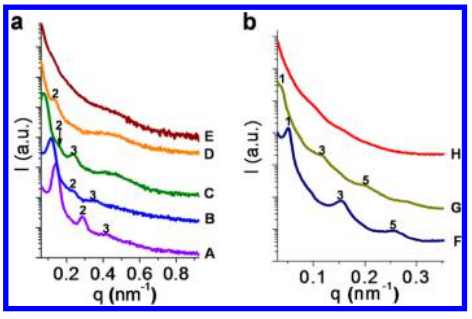

Figure 1. (a) SAXS profiles of BBCP **A**, **B**, **C**, **D**, and **E** showing the increased *d*-spacing with the increased molecular weight. (b) Synchrotron SAXS profiles of BBCP **F**, **G**, and **H** showing large *d*-spacing over 100 nm.

DOI: 10.1021/acs.macromol.6b00926
Macromolecules 2016, 49, 5068−5075

periodic nanostructure with a domain spacing of approximately 123 nm ($d_s = 2\pi/q$). A well-ordered lamellar structure was confirmed by the higher-order reflections located at $3q$ and $5q$. As shown in Figure 1, a systematic shift of the scattering vector of the first- and higher-order peaks to smaller q regions was observed with increasing BBCP molecular weight, indicating the expected increase of the domain spacing from 43.6 to 185 nm (see Table 1). For BBCP **D**, the domain spacing was estimated based on the second-order peak. Transmission electron microscopy (TEM) was also employed to verify the lamellar morphologies, and TEM micrographs (Figure S1, Supporting Information) of the stained samples prepared by microtoming further confirmed the well-ordered lamellar morphologies, consistent with the SAXS data. For BBCP **E** and **H**, no evident peaks can be identified in the SAXS data (Figure 1). The morphology and domain spacing of the samples were obtained by analysis of TEM micrographs in Figure S1d,e.

Cadmium selenide (CdSe) NPs from QD Vision Inc. were initially capped by trioctylphosphine oxide (TOPO) and dispersed in a nonpolar solvent. To enhance the interaction between the NPs and the PEO block of PS-*b*-PEO BBCPs, surface modification was performed to replace the original ligands with 11-mercaptoundecylhydroquinone through an effective ligand-exchange process (see Experimental Section for details). The resulting product was despersible in tetrahydrofuran (THF), and the solution was stable for more than 6 months. The strong vibration absorption of the hydroquinone group at 3362 cm^{-1} was observed in the FTIR spectrum (Figure S2) of the modified NPs after purification, indicating the ligand was successfully adsorbed on the surface of the QDs. The inorganic content represents approximately 81 wt % of the QDs according to thermogravimetric analysis (TGA) (Figure S3). The mean diameter of the NP core (9.7 ± 1.6 nm) shown in the inset histogram was obtained from image analysis based on a TEM micrograph (Figure 2) for at least 400 NPs using ImageJ. The ligand used here is not only an effective stabilizer for the QDs but also a hydrogen donor that exhibits strong hydrogen-bonding interactions with the PEO side chains of the PS-*b*-PEO BBCPs.

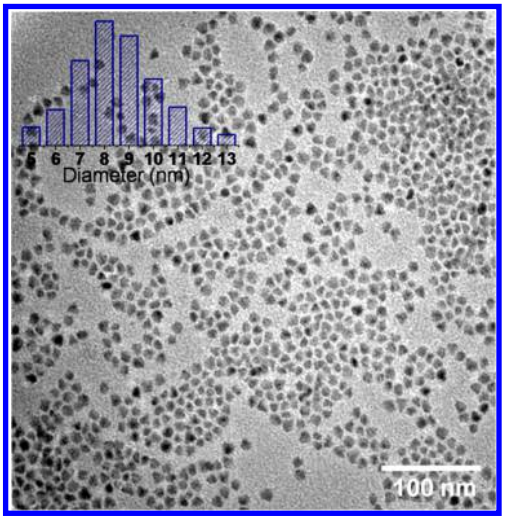

Figure 2. TEM micrograph of CdSe NPs capped with 11-mercaptoundecylhydroquinone and the size distribution (inset). The average core diameter is 9.7 ± 1.6 nm obtained by image analysis using ImageJ.

For the BBCP−NP composites, we typically prepared a 2% (w/v) polymer solution in anhydrous tetrahydrofuran (THF) admixed with QD NPs with different weight fractions. Herein the weight percentage (wt %) of NPs in the composites is based on the mass of the NP core and ligand shell, while the volume percentage (vol %) of NPs (core + ligand) can be estimated using the TGA data and the densities of the components and is provided in parentheses following the first mention of the NP wt % for each composites (see calculation details in Supporting Information). Briefly, the composite films were obtained simply by casting and evaporation of the mixture solutions on horizontal glass substrates. Solvent annealing was carried out on the resulting composite films in saturated dichloromethane (DCM) vapor for 2 days. Humidity was found to influence on the morphology of these nanocomposites template by the amphiphilic BBCPs. Consequently, we controlled the humidity to levels below 20% using a nitrogen atmosphere during the evaporation of the solvent to minimize any influence of moisture.

The nanocomposites were prepared from blends of selected BBCPs in Table 1 with the QDs at different loading percentages: 15 wt % (6.6 vol %) or 30 wt % (15 vol %). SAXS measurements were performed using synchrotron light sources, and a gradual decrease of the q vector of the primary order peak was observed in the SAXS data (Figure 3) of the

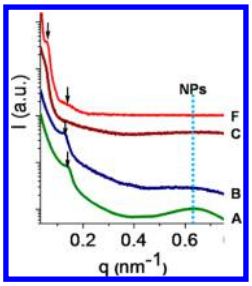

Figure 3. SAXS profiles of blends of CdSe NPs (15 wt %, 6.6 vol %) within the BBCPs of different molecular weights: **A** (160 kg/mol), **B** (185 kg/mol), **C** (285 kg/mol), and **F** (995 kg/mol).

nanocomposites containing 15 wt % of the QDs, indicating the domain spacing increased with the increase of the molecular weight. However, no higher-order peaks can be identified due to the strong X-ray scattering background from the large NPs (~9.7 nm). The morphology of the composites was confirmed by TEM and field emission scanning electron microscopy (FESEM). Well-ordered lamellar morphologies of QD arrays were observed as indicated by the TEM micrographs of microtomed thin sections of these composites (see Figure 4a−h). We note that since PS and PEO of the unstained samples have similar electron densities, the contrast observed in the TEM is evidently due to QDs residing exclusively in PEO domains. The formation of multiple hydrogen bonds between QD ligands and PEO brushes enabled the precise control and selective incorporation of QDs into the PEO domain of the phase-separated BBCPs. TEMs of nanocomposites containing 15 wt % of the QDs are shown in Figure 4a−e, and the domain spacing between QD layers increased from 46.2 to 100 nm with the increased molecular weight of BBCP from 160 to 995 kg/mol. As shown in Figure 4f−h, well-ordered lamellar morphologies were maintained for nanocomposites containing

DOI: 10.1021/acs.macromol.6b00926
Macromolecules 2016, 49, 5068−5075

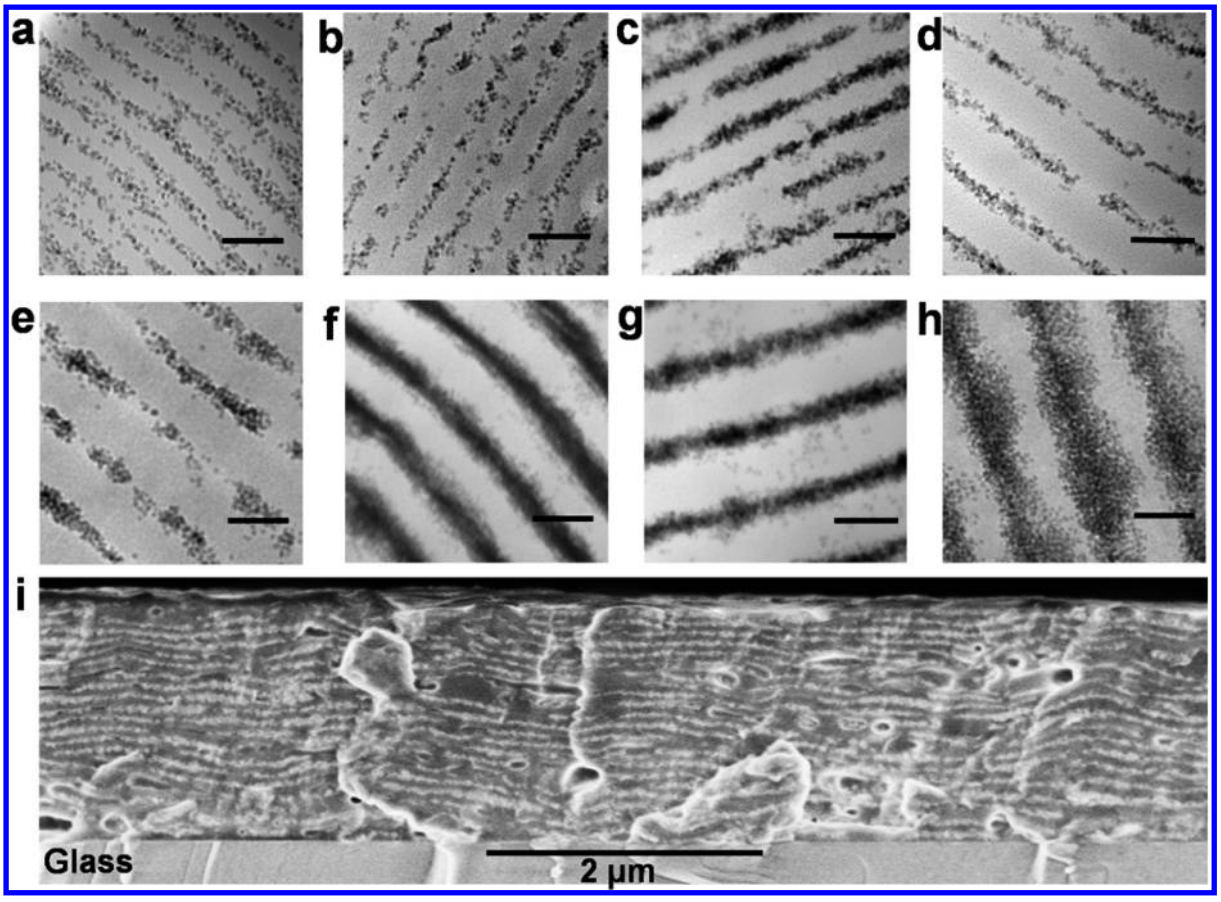

Figure 4. Directed assembly of CdSe NPs in BBCPs through hydrogen-bonding interactions between the ligands on NPs and PEO brushes of the BBCPs. TEM micrographs (a–e) are blends of the QDs (15 wt %, 6.6 vol %) with the brush BCPs of different molecular weights: (a) **A** (160 kg/mol); (b) **B** (185 kg/mol); (c) **C** (285 kg/mol); (d) **E** (487 kg/mol); (e) **F** (995 kg/mol). TEM micrographs (f–h) are blends of the QDs (30 wt %, 15 vol %) with the BBCPs of various molecular weights: (f) **D** (374 kg/mol); (g) **E** (487 kg/mol); (h) **G** (1150 kg/mol). The scale bars correspond to 100 nm for all the TEM micrographs. The domain spacing of the nanocomposites was estimated based on the analysis of the TEM micrographs: (a) 46.2, (b) 51.1, (c) 68.2, (d) 86.7, (e) 100, (f) 94.6, (g) 99.8, and (h) 145 nm. (i) Cross-sectional FESEM micrograph of the composite film (BBCP **D**) with the QDs (30 wt %) appearing as the bright regions.

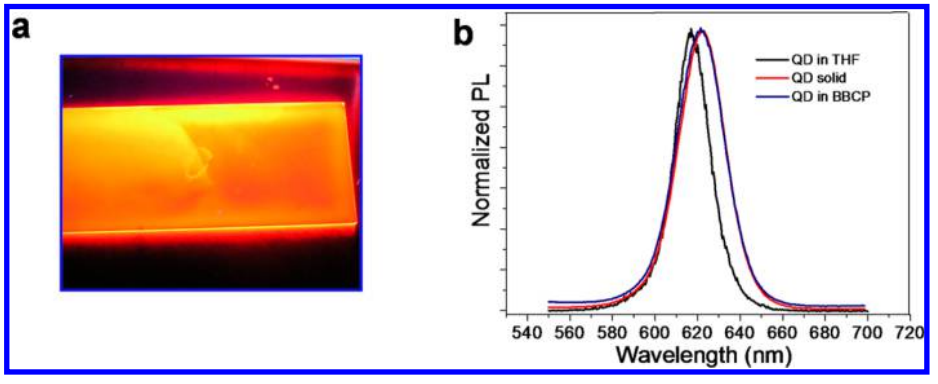

Figure 5. (a) Photograph of a composite film under the UV light (365 nm) for the blend of BBCP **D** with 30 wt % QDs. (b) Photoluminescence (PL) spectra of QDs dispersed in THF (black), solid (red), and BBCP **D** (blue). The wavelength of light for excitation was 365 nm.

30 wt % of the QDs, and a large domain spacing of up to 145 nm was observed using BBCP **G** (1150 kg/mol) as the template (Figure 4h). For the composite samples based on the same polymer matrix (BBCP **D**), the domain spacing increased from 86.7 to 99.8 nm with an increase of NP loading from 15 to 30 wt % (Figure 4d vs 4g), suggesting swelling of the PEO domains by the NP additives. TEM micrographs (Figure S4) at lower magnifications further confirmed the well-ordered lamellar structure formed in large areas. Moreover, Figure 4i shows the cross-sectional FESEM of a composite film containing 30 wt % of the QDs. QD layered structure parallel to the glass substrate was observed with the QD layers appearing as the bright regions consistent with the TEM result (Figure 4f).

Significantly different from the coil-like LBCP, the molecular backbone of a BBCP is highly stretched due to steric congestion deriving from the densely grafted polymer side chains, resulting in fewer polymer chain entanglements relative

DOI: 10.1021/acs.macromol.6b00926
Macromolecules 2016, 49, 5068–5075

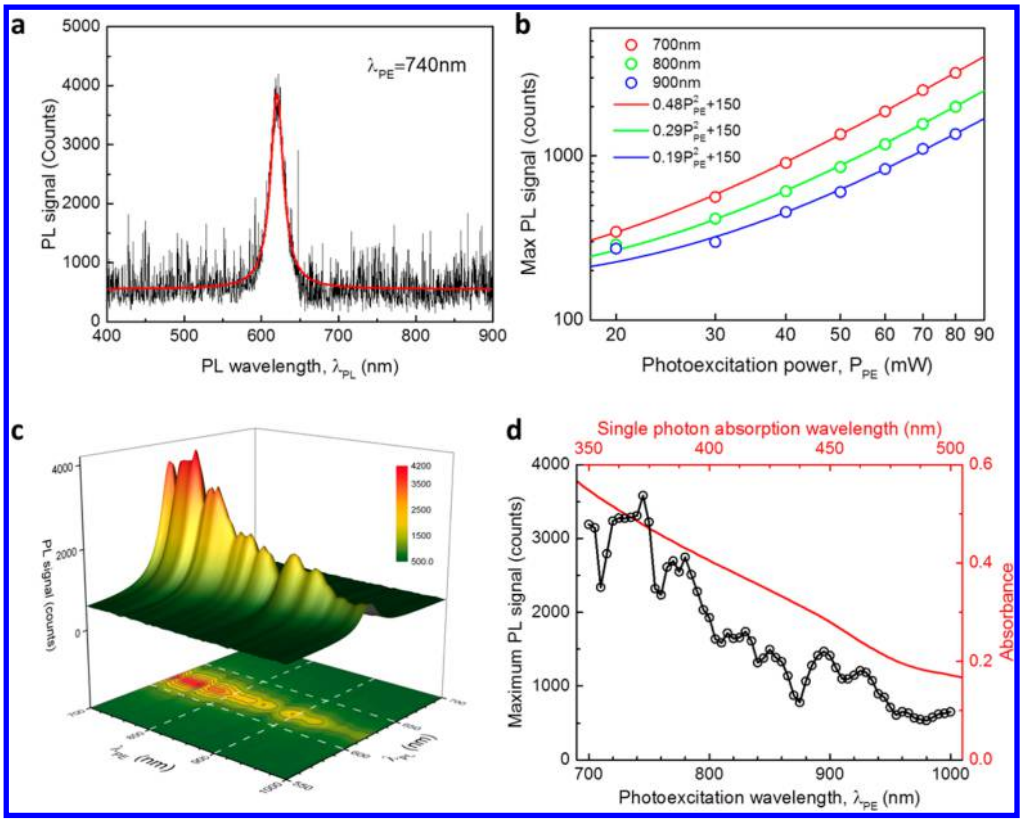

Figure 6. TP-PL of the blend of BBCP **D** with 30 wt % QDs. (a) A TP-PL spectrum for 740 nm wavelength photoexcitation at P_{PE} = 80 mW. The red line shows a Lorentzian fitting curve. (b) P_{PE}-dependent TP-PL signals at the peak of PL spectra for the three selected λ_{PE} values (circles) are shown with the corresponding fitting curves (lines). (c) PL spectra are plotted depending on λ_{PE} at a fixed P_{PE} value of 80 mW. (d) One-photon absorption spectrum (red) and maximum PL intensity as a function of excitation wavelength.

to their linear analogues.[35−43] This enables their rapid self-assembly to yield nanostructures with larger domains and consequently enhances the capabilities of these BCPs for accommodating large NPs at high loading percentages.[43] We also note the successful incorporation of the QDs (9.7 nm) into a PEO microdomain of only 18 nm as indicated by Figure 4a with a $d/L_{PEO} > 0.54$, where d is the average core diameter of the QDs and L_{PEO} is the width of the PEO domain as calculated based on the volume fraction of PEO (f_{PEO}) and the domain spacing (d_s) of the neat polymer ($L_{PEO} = d_s \times f_{PEO}$). For comparison, the d/L values in well-ordered nanocomposites based on LBCPs have been generally limited to less than 0.3.[15−33] The strong hydrogen-bonding interactions between the NP ligands and the PEO side chains play an important role in the creation of the highly ordered BCP nanocomposites through a supramolecular self-assembly process. The BBCP-based nanocomposites with high loadings of the functionalities arranged in well-ordered nanostructures with widely tunable lattice parameters provide novel polymer hybrid materials with unique electric or optical properties such as strong nonlinear optical responses (see below).

The composite sample containing BBCP **D** and 30 wt % of QDs was chosen as a model system for the subsequent investigation of optical properties. TEM (Figure 4f) and cross-sectional FESEM (Figure 4i) confirmed the arrangements of QD arrays into a well-ordered lamellar morphology with a long-range order parallel to the glass substrate. As shown in Figure 5a, strong red emission was observed from the well-ordered QD arrays under UV light (365 nm). The photoluminescence (PL) of the QDs was recorded on a fluorescence spectrometer. Figure 5b shows the PL spectra of the QDs in THF solution, in solid, and in the QD/BBCP blend. The QD solution emitted red light with an intensity maximum at 616 nm. In comparison, a slight red-shift of the peak to approximately 620 nm was observed for both the QDs solid and the QD/BBCP blend due to coupling between adjacent QD NPs and/or different chemical environments.[53]

Figure 6a is the two-photon photoluminescence (TP-PL) spectrum when the blend of BBCP **D** with 30 wt % QDs was excited by 740 nm wavelength femtosecond (fs) pulses at a photoexcitation power (P_{PE}) of 80 mW. The measured TP-PL spectra (black line) were fit with a Lorentzian function (red line) for the quantification of the TP-PL spectra. The full width at half-maximum (fwhm) of the TP-PL spectra was approximately 19 nm, which is similar to that in Figure 5b. Figure 6b shows the PL spectra versus P_{PE} for three selected photoexcitation wavelengths (λ_{PE}) and quadratic fitting curves with a constant background signal of 150. The measured maximum TP-PL signal is clearly proportional to the square of P_{PE}, and this quadratic nonlinearity evidently shows that the QDs were excited through two-photon absorption (TPA). To demonstrate the optimal λ_{PE}, the blend of BBCP-D with 30 wt % QDs was photoexcited in a broad range of λ_{PE} (700−1000 nm) with a fixed P_{PE} (80 mW). Although the general trend of PL signal follows the single-photon absorption spectrum (Figure 6d and Figure S5), several peaks corresponding to different transitions based on the selection rules (Δm = 0, ±1) are observed,[54] where m is the azimuthal angular momentum. The peak TP-PL signal (or the largest TP cross section) was observed at λ_{PE} = 740 nm (equivalent to 1.68 eV) for the range

DOI: 10.1021/acs.macromol.6b00926
Macromolecules 2016, 49, 5068−5075

of λ_{PE}. We also investigated the multiphoton excitation fluorescence (FL) of the composite sample using a multiphoton microscope with a fs light source. The equipment configuration is depicted in the Experimental Section and previous publications.[55,56] The laser beam is at 1550 nm with a repetition rate of 75 MHz and pulse duration of 150 fs. Figure 7a demonstrates the normalized multiphoton excitation

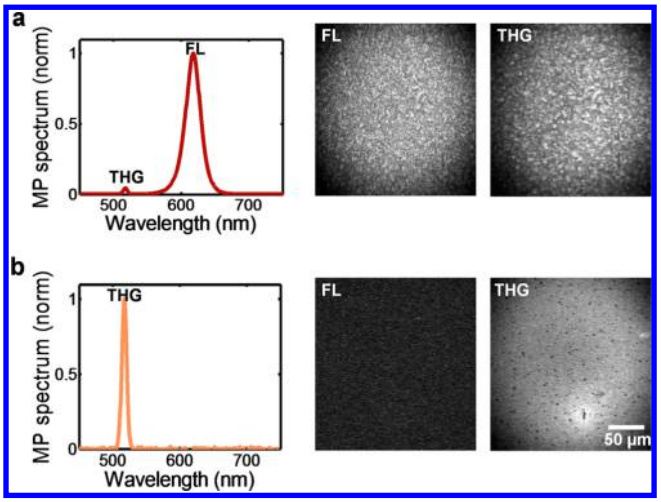

Figure 7. Normalized multiphoton excitation spectra and micrographs of (a) the blend of BBCP **D** with 30 wt % QDs and (b) neat polymer sample. The wavelength of light for excitation was 1550 nm.

spectrum of the blend of BBCP **D** with 30 wt % QDs. The sample shows a strong FL signal at ~620 nm and a third harmonic generation (THG) peak at ~517 nm. The FL signal observed from the well-ordered QD arrays was induced by three-photon absorption of the laser light at 1550 nm, indicating the potential use of the well-ordered composite films as coatings for nonlinear optics. It should be noted that the multiphoton spectrum of the neat polymer sample shows THG but no FL signal (Figure 7b). Therefore, almost all the FL signal is generated from the arrays of QDs rather than the polymer matrix.

The copolymer's contribution to the observed THG signals of the measured samples is non-negligible. By direct comparison of the multiphoton microscope THG signal with that of the standard BK7 glass, a well-known reference, we can estimate values of third-order susceptibility ($\chi^{(3)}$).[55] It should be noted that the estimations are based on a value of $\chi^{(3)}(-3\omega;\omega,\omega,\omega) = 5 \times 10^{-14}$ esu for BK-7 glass.[57] In addition to the THG intensity, the determination of sample thickness (3.8 μm) and linear optical properties ($n_{517\,nm}$ = 1.57 and $n_{1550\,nm}$ = 1.55, by ellipsometry shown in Figure S6) also affect the determination of $\chi^{(3)}(-3\omega;\omega,\omega,\omega)$. We find that the values of the THG third-order susceptibility are quite large, 7.8×10^{-11} esu, which is about 1500 times larger than the reference, indicating that the composites may be promising materials for nonlinear optics.

CONCLUSION

The directed assembly of QD arrays into well-ordered lamellar structures was achieved using a series of PS-*b*-PEO BBCPs as the templates affording novel hybrid materials containing a high loading of up to 30 wt % (15 vol %) functionalities. Compared with the nanocomposites based on LBCPs, a broad lattice spacing of the well-ordered QD arrays from 46.5 to 145 nm was realized simply by changing the molecular weight of the BBCP matrix. Moreover, the BBCPs exhibited enhanced capability for the accommodation of large NPs as indicated by the successful incorporation of the QDs (9.7 nm) into a PEO microdomain of only 18 nm in width ($d/L_{PEO} > 0.54$). For comparison, the d/L values have been generally limited to less than 0.3 for the well-ordered nanocomposites based on LBCPs. Femtosecond laser light at various wavelengths from 700 to 1550 nm was employed in a systematic investigation of the nonlinear optical properties of the well-ordered QD arrays, and strong PL as well as THG was observed via multiphoton excitation. This work provides a simple strategy for the creation of well-ordered photonic nanocomposites with widely tunable lattice parameters which may be useful in nonlinear optical applications

EXPERIMENTAL SECTION

Surface Modification of CdSe Nanoparticles. The ligand of CdSe received was trioctylphosphine oxide, which was exchanged according to the modified procedure in refs 58 and 59. 0.5 mL of CdSe QDs dispersed in toluene (~100 mg/mL) was dried in a nitrogen flow and redispersed in 10 mL of anhydrous hexane. The hexane dispersion was mixed with 10 mL of anhydrous acetonitrile and was combined with 0.25 mL of dichloromethane solution of Et_3OBF_4 (1 M) at room temperature. The resulting mixture was shaken until the CdSe NPs were transferred from the upper hexane layer to the bottom acetonitrile layer. The NPs were purified by centrifugation (15 000 rpm, 15 min) and redispersed in THF (20 mL).

The Et_3OBF_4-treated CdSe NPs can be further stabilized by various ligands, through secondary ligand exchange reaction. 10 mL of THF solution of CdSe (~5 mg/mL) previously synthesized was added 0.2 g of 11-mercaptoundecylhydroquinone. The resulting solution was stirred at room temperature for 3 days. The surface-modified NPs were precipitated and purified by centrifugation (15 000 rpm, 5 min) and then redispersed in THF (~10 mg/mL).

Composite Sample Preparation. Appropriate amounts of BBCPs were weighed and dissolved in anhydrous tetrahydrofuran (THF) followed by adding nanoparticle solutions to form 2% (w/v) stock solutions. The THF solutions were poured through a 0.45 μm filter onto horizontal glass substrates and covered immediately with glass Petri dishes. The films after evaporation for about 4 h were annealed in saturated dichloromethane (DCM) vapor for 2 days. We note that the evaporation of THF solutions was carried out in a nitrogen atmosphere to control humidity below 20%.

Two-Photon Excitation Fluorescence Measurement. Two-photon photoluminescence (TP-PL) measurements were performed using 100 fs pulses generated by a Ti:sapphire oscillator (Mai Tai HP, Spectra-Physics) with a tuning range of 690−1040 nm and a repetition rate of 80 MHz. The pulses (a beam diameter of 1.2 mm) were focused by a convex lens (f = 40 mm), and the sample was placed at 2 mm from the focal point, in order to get enough intensity for TP-PL. The TP-PL was collected by another convex lens (f = 40 mm) and coupled to an optical fiber to feed into a spectrometer (Flame-VIS-NIR, Ocean Optics), while blocking the excitation pulses by a 680 nm blocking edge short-pass emission filter (optical density >8, Semrock).

Multiphoton Excitation Fluorescence and Third Harmonic Generation Measurements. A multiphoton microscope with a femtosecond (fs) light source was employed to measure the multiphoton excitation fluorescence. The experimental configuration is depicted in previous publications.[55,56] The laser beam is at 1550 nm with a repetition rate of 75 MHz and pulse duration of 150 fs. The input femtosecond laser beam is raster scanned across the sample using a two-dimensional galvo-scanner system. The beam is relayed and expanded with a scan lens and a tube lens arranged in a telescopic scheme. The back aperture of the objective is fully illuminated to make use of the full NA (NA = 0.5, 20× aspheric objective lens) and create the smallest possible laser spot size on the sample (confocal parameter = 6 μm, spot size = 1.6 μm). The backscattered signals are detected simultaneously using two highly sensitive high gain PMTs through a

DOI: 10.1021/acs.macromol.6b00926
Macromolecules 2016, 49, 5068−5075

series of dichroic beam splitters and filters. The fluorescence due to two- or three-photon excitation can be measured by removing the 780 nm bandpass filter or 520 nm bandpass filter from the transmission path of dichroic mirror. The generated multiphoton signals can also be detected with a sensitive spectrometer with the use of a rotating dichroic mirror at 870 nm.

Characterization. Small-angle X-ray scattering (SAXS) measurements were performed using an Rigaku-Molecular Metrology SAXS equipment with a 0.154 nm (Cu K radiation) X-ray beam, and the sample-to-detector distance was 1467 mm. SAXS measurements were also performed using the SAXS instrument at the Shanghai Synchrotron Radiation Facility (SSRF). The energy of incident X-ray was 10 keV (0.124 nm), and the sample-to-detector distance was 5100 mm. Transmission electron microscopy (TEM) measurements were conducted with a JEOL 2000FX TEM operated at accelerating voltages of 200 kV. Brush BCPs as well as the composites samples were embedded in epoxy and cured at room temperature overnight. Thin sections of approximately 50 nm in thickness for microscopy were prepared using a Leica Ultracut UCT microtome equipped with a Leica EM FCS cryogenic sample chamber operated at −80 °C. Field emission scanning electron microscopy (FESEM) measurements were carried out on a FEI Magellan 400 FESEM. The composite sample was cryofractured in liquid nitrogen to afford the cross sections for SEM. Fourier transform infrared spectroscopy (FTIR) was performed on a Bruker Vertex 70 FTIR spectrophotometer. Thermogravimetric analysis (TGA) experiments were performed on a TGA2950 thermogravimetric analyzer with a heating rate of 10 °C/min under a N_2 atmosphere. Photoluminescence of QDs was measured using a PerkinElmer LS 55 fluorescence spectrometer.

■ ASSOCIATED CONTENT

Supporting Information

The Supporting Information is available free of charge on the ACS Publications website at DOI: 10.1021/acs.macromol.6b00926.

TEM images of the brush block copolymers; FTIR spectrum and TGA of cadmium selenide nanoparticles; TEM images, absorption, and VASE spectrum of nanocomposites (PDF)

■ AUTHOR INFORMATION

Corresponding Authors

*E-mail watkins@polysci.umass.edu; Tel 413-545-2569; Fax 413-545-0082 (J.J.W.).

*E-mail rnorwood@optics.arizona.edu; Tel 520-626-0936 (R.A.N.).

*E-mail leejh@umass.edu; Tel (413) 545−0667 (J.-H.L.).

Notes

The authors declare no competing financial interest.

■ ACKNOWLEDGMENTS

The authors acknowledge the use of the Advanced Light Source at the Shanghai Synchrotron Radiation Facility (SSRF). This work was supported by the NSF Center for Hierarchical Manufacturing at the University of Massachusetts (CMMI-1025020).

■ REFERENCES

(1) Bockstaller, M. R.; Mickiewicz, R. A.; Thomas, E. L. Block Copolymer Nanocomposites: Perspectives for Tailored Functional Materials. *Adv. Mater.* **2005**, *17*, 1331−1349.

(2) Orilall, M. C.; Wiesner, U. Block Copolymer Based Composition and Morphology Control in Nanostructured Hybrid Materials for Energy Conversion and Storage: Solar Cells, Batteries, and Fuel Cells. *Chem. Soc. Rev.* **2011**, *40*, 520−535.

(3) Kao, J.; Thorkelsson, K.; Bai, P.; Rancatoreb, B. J.; Xu, T. Toward Functional Nanocomposites: Taking the Best of Nanoparticles, Polymers, and Small Molecules. *Chem. Soc. Rev.* **2013**, *42*, 2654−2678.

(4) Sarkar, B.; Alexandridis, P. Block Copolymer−Nanoparticle Composites: Structure, Functional Properties, and Processing. *Prog. Polym. Sci.* **2015**, *40*, 33−62.

(5) Stefik, M.; Guldin, S.; Vignolini, S.; Wiesner, U.; Steiner, U. Block Copolymer Self-Assembly for Nanophotonics. *Chem. Soc. Rev.* **2015**, *44*, 5076−5091.

(6) Choi, C. L.; Alivisatos, A. P. From Artificial Atoms to Nanocrystal Molecules: Preparation and Properties of More Complex Nanostructures. *Annu. Rev. Phys. Chem.* **2010**, *61*, 369−389.

(7) Talapin, D. V.; Lee, J.-S.; Kovalenko, M. V.; Shevchenko, E. V. Prospects of Colloidal Nanocrystals for Electronic and Optoelectronic Applications. *Chem. Rev.* **2010**, *110*, 389−458.

(8) Huynh, W. U.; Dittmer, J. J.; Alivisatos, A. P. Hybrid Nanorod-Polymer Solar Cells. *Science* **2002**, *295*, 2425−2427.

(9) Lopes, W. A.; Jaeger, H. M. Hierarchical Self-Assembly of Metal Nanostructures on Diblock Copolymer Scaffolds. *Nature* **2001**, *414*, 735−738.

(10) De Rosa, C.; Auriemma, F.; Di Girolamo, R.; Pepe, G. P.; Napolitano, T.; Scaldaferri, R. Enabling Strategies in Organic Electronics Using Ordered Block Copolymer Nanostructures. *Adv. Mater.* **2010**, *22*, 5414−5419.

(11) Xiang, J.; Lu, W.; Hu, Y.; Wu, Y.; Yan, H.; Lieber, C. M. Ge/Si Nanowire Heterostructures as High-Performance Field-Effect Transistors. *Nature* **2006**, *441*, 489−493.

(12) Briseno, A. L.; Yang, P. Optoelectronics: Combining Chemical Worlds. *Nat. Mater.* **2009**, *8*, 7−8.

(13) Lin, Y.; Lim, J. A.; Wei, Q.; Mannsfeld, S. C. B.; Briseno, A. L.; Watkins, J. J. Cooperative Assembly of Hydrogen-Bonded Diblock Copolythiophene/Fullerene Blends for Photovoltaic Devices with Well-Defined Morphologies and Enhanced Stability. *Chem. Mater.* **2012**, *24*, 622−632.

(14) Wei, Q. S.; Lin, Y.; Anderson, E. R.; Briseno, A. L.; Gido, S. P.; Watkins, J. J. Additive-Driven Assembly of Block Copolymer−Nanoparticle Hybrid Materials for Solution Processable Floating Gate Memory. *ACS Nano* **2012**, *6*, 1188−1194.

(15) Lee, J. Y.; Thompson, R. B.; Jasnow, D.; Balazs, A. C. Entropically Driven Formation of Hierarchically Ordered Nanocomposites. *Phys. Rev. Lett.* **2002**, *89*, 155503.

(16) Bockstaller, M. R.; Lapetnikov, Y.; Margel, S.; Thomas, E. L. Size-Selective Organization of Enthalpic Compatibilized Nanocrystals in Ternary Block Copolymer/Particle Mixtures. *J. Am. Chem. Soc.* **2003**, *125*, 5276−5277.

(17) Chiu, J. J.; Kim, B. J.; Kramer, E. J.; Pine, D. J. Control of Nanoparticle Location in Block Copolymers. *J. Am. Chem. Soc.* **2005**, *127*, 5036−5037.

(18) Lin, Y.; Böker, A.; He, J. B.; Sill, K.; Xiang, H. Q.; Abetz, C.; Li, X. F.; Wang, J.; Emrick, T.; Long, S.; Wang, Q.; Balazs, A.; Russell, T. P. Self-Directed Self-Assembly of Nanoparticle/ Copolymer Mixtures. *Nature* **2005**, *434*, 55−59.

(19) Balazs, A. C.; Emrick, T.; Russell, T. P. Nanoparticle Polymer Composites: Where Two Small Worlds Meet. *Science* **2006**, *314*, 1107−1110.

(20) Kim, B. J.; Chiu, J. J.; Yi, G. R.; Pine, D. J.; Kramer, E. J. Nanoparticle-Induced Phase Transitions in Diblock-Copolymer Films. *Adv. Mater.* **2005**, *17*, 2618−2622.

(21) Kim, B. J.; Bang, J.; Hawker, C. J.; Kramer, E. J. Effect of Areal Chain Density on the Location of Polymer-Modified Gold Nanoparticles in A Block Copolymer Template. *Macromolecules* **2006**, *39*, 4108−4114.

(22) Kim, B. J.; Bang, J.; Hawker, C. J.; Chiu, J. J.; Pine, D. J.; Jang, S. G.; Yang, S. M.; Kramer, E. J. Creating Surfactant Nanoparticles for Block Copolymer Composites Through Surface Chemistry. *Langmuir* **2007**, *23*, 12693−12703.

(23) Chiu, J. J.; Kim, B. J.; Yi, G. R.; Bang, J.; Kramer, E. J.; Pine, D. J. Distribution of Nanoparticles in Lamellar Domains of Block Copolymers. *Macromolecules* **2007**, *40*, 3361−3365.

DOI: 10.1021/acs.macromol.6b00926
Macromolecules 2016, 49, 5068−5075

(24) Kim, B. J.; Fredrickson, G. H.; Kramer, E. J. Effect of Polymer Ligand Molecular Weight on Polymer-Coated Nanoparticle Location in Block Copolymers. *Macromolecules* **2008**, *41*, 436−447.
(25) Jang, S. G.; Kramer, E. J.; Hawker, C. J. Controlled Supramolecular Assembly of Micelle-Like Gold Nanoparticles in PS-b-P2VP Biblock Copolymers *via* Hydrogen Bonding. *J. Am. Chem. Soc.* **2011**, *133*, 16986−16996.
(26) Lin, Y.; Daga, V. K.; Anderson, E. R.; Gido, S. P.; Watkins, J. J. Nanoparticle-Driven Assembly of Block Copolymers: A Simple Route to Ordered Hybrid Materials. *J. Am. Chem. Soc.* **2011**, *133*, 6513−6516.
(27) Jang, S. G.; Khan, A.; Hawker, C. J.; Kramer, E. J. Morphology Evolution of PS-b-P2VP Diblock Copolymers *via* Supramolecular Assembly of Hydroxylated Gold Nanoparticles. *Macromolecules* **2012**, *45*, 1553−1561.
(28) Yao, L.; Lin, Y.; Watkins, J. J. Ultra High Loading of Nanoparticles into Ordered Block Copolymer Composites. *Macromolecules* **2014**, *47*, 1844−1849.
(29) Song, D. P.; Wang, X.; Lin, Y.; Watkins, J. J. Synthesis and Controlled Self-Assembly of UV-Responsive Gold Nanoparticles in Block Copolymer Templates. *J. Phys. Chem. B* **2014**, *118*, 12788−12795.
(30) Zhao, Y.; Thorkelsson, K.; Mastroianni, A. J.; Schilling, T.; Luther, J. M.; Rancatore, B. J.; Matsunaga, K.; Jinnai, H.; Wu, Y.; Poulsen, D.; Fréchet, J. M. J.; Alivisatos, A. P.; Xu, T. Small-Molecule-Directed Nanoparticle Assembly towards Stimuli-Responsive Nanocomposites. *Nat. Mater.* **2009**, *8*, 979−985.
(31) Kao, J.; Bai, P.; Lucas, J. M.; Alivisatos, A. P.; Xu, T. Size-Dependent Assemblies of Nanoparticle Mixtures in Thin Films. *J. Am. Chem. Soc.* **2013**, *135*, 1680−1683.
(32) Kao, J.; Xu, T. Nanoparticle Assemblies in Supramolecular Nanocomposite Thin Films: Concentration Dependence. *J. Am. Chem. Soc.* **2015**, *137*, 6356−6365.
(33) Warren, S. C.; Messina, L. C.; Slaughter, L. S.; Kamperman, M.; Zhou, Q.; Gruner, S. M.; DiSalvo, F. J.; Wiesner, U. Ordered Mesoporous Materials from Metal Nanoparticle-Block Copolymer Self-Assembly. *Science* **2008**, *320*, 1748−1752.
(34) Runge, M. B.; Bowden, N. B. Synthesis of High Molecular Weight Comb Block Copolymers and Their Assembly into Ordered Morphologies in the Solid State. *J. Am. Chem. Soc.* **2007**, *129*, 10551−10560.
(35) Rzayev, J. Molecular Bottlebrushes: New Opportunities in Nanomaterials Fabrication. *ACS Macro Lett.* **2012**, *1*, 1146−1149.
(36) Rzayev, J. Synthesis of Polystyrene−Polylactide Bottlebrush Block Copolymers and Their Melt Self-Assembly into Large Domain Nanostructures. *Macromolecules* **2009**, *42*, 2135−2141.
(37) Xia, Y.; Olsen, B. D.; Kornfield, J. A.; Grubbs, R. H. Efficient Synthesis of Narrowly Dispersed Brush Copolymers and Study of Their Assemblies: The Importance of Side Chain Arrangement. *J. Am. Chem. Soc.* **2009**, *131*, 18525−18532.
(38) Bolton, J.; Bailey, T. S.; Rzayev, J. Large Pore Size Nanoporous Materials from the Self-Assembly of Asymmetric Bottlebrush Block Copolymers. *Nano Lett.* **2011**, *11*, 998−1001.
(39) Sveinbjörnsson, B. R.; Weitekamp, R. A.; Miyake, G. M.; Xia, Y.; Atwater, H. A.; Grubbs, R. H. Rapid Self-Assembly of Brush Block Copolymers to Photonic Crystals. *Proc. Natl. Acad. Sci. U. S. A.* **2012**, *109*, 14332−14336.
(40) Macfarlane, R. J.; Kim, B.; Lee, B.; Weitekamp, R. A.; Bates, C. M.; Lee, S. F.; Chang, A. B.; Delaney, K. T.; Fredrickson, G. H.; Atwater, H. A.; Grubbs, R. H. Improving Brush Polymer Infrared One-Dimensional Photonic Crystals *via* Linear Polymer Additives. *J. Am. Chem. Soc.* **2014**, *136*, 17374−17377.
(41) Song, D.-P.; Li, C.; Colella, N. S.; Xie, W.; Li, S.; Lu, X.; Gido, S.; Lee, J.-H.; Watkins, J. J. Large Volume Self-Organization of Polymer/Nanoparticle Hybrids with Millimeter Scale Grain Sizes Using Brush Block Copolymers. *J. Am. Chem. Soc.* **2015**, *137*, 12510−12513.
(42) Song, D.-P.; Li, C.; Colella, N. S.; Lu, X.; Lee, J.-H.; Watkins, J. J. Metallodielectric Photonic Crystals from the Self-Assembly of Brush Block Copolymers and Gold Nanoparticles. *Adv. Opt. Mater.* **2015**, *3*, 1169−1175.
(43) Song, D.-P.; Lin, Y.; Gai, Y.; Colella, N. S.; Li, C.; Liu, X.-H.; Gido, S.; Watkins, J. J. Controlled Supramolecular Self-Assembly of Large Nanoparticles in Amphiphilic Brush Block Copolymers. *J. Am. Chem. Soc.* **2015**, *137*, 3771−3774.
(44) Nozik, A. J.; Beard, M. C.; Luther, J. M.; Law, M.; Ellingson, R. J.; Johnson, J. C. Semiconductor Quantum Dots and Duantum Dot Arrays and Applications of Multiple Exciton Generation to Third-Generation Photovoltaic Solar Cells. *Chem. Rev.* **2010**, *110*, 6873−6890.
(45) Petruska, M. A.; Malko, A. V.; Voyles, P. M.; Klimov, V. I. High-Performance, Quantum Dot Nanocomposites for Nonlinear Optical and Optical Gain Applications. *Adv. Mater.* **2003**, *15*, 610−613.
(46) Qian, G.; Lin, Y.; Wantz, G.; Davis, A. R.; Carter, K. R.; Watkins, J. J. Saturated and Multi-Colored Electroluminescence from Quantum Dots Based Light Emitting Electrochemical Cells. *Adv. Funct. Mater.* **2014**, *24*, 4484−4490.
(47) Lee, J.-H.; Koh, C. Y.; Singer, J. P.; Jeon, S.-J.; Maldovan, M.; Stein, O.; Thomas, E. L. 25th Anniversary Article: Ordered Polymer Structures for the Engineering of Photons and Phonons. *Adv. Mater.* **2014**, *26*, 532−569.
(48) Kopp, V. T.; Fan, B.; Vithana, H. K. M.; Genack, A. Z. Low-Threshold Lasing at the Edge of A Photonic Stop Band in Cholesteric Liquid Crystals. *Opt. Lett.* **1998**, *23*, 1707−1709.
(49) Kyu, H.-Y.; Kim, S. H.; Lee, Y. J.; Lee, Y. H. Very-Low Threshold Photonic Band-Edge Lasers from Free Standing Triangular Photonic Crystal Slabs. *Appl. Phys. Lett.* **2002**, *80*, 3476−3478.
(50) Min, K.; Choi, Y.-K.; Jeon, H. Model Calculations for Enhanced Fluorescence in Photonic Crystal Phosphor. *Opt. Express* **2012**, *20*, 2452−2459.
(51) Xing, G.; Liao, Y.; Wu, X.; Chakrabortty, S.; Liu, X.; Yeow, E. K. L.; Chan, Y.; Sum, T. C. Ultralow-Threshold Two-Photon Pumped Amplified Spontaneous Emission and Lasing from Seeded CdSe/CdS Nanorod Heterostructures. *ACS Nano* **2012**, *6*, 10835−10844.
(52) Li, M.; Zhi, M.; Zhu, H.; Wu, W.-Y.; Xu, Q.-H.; Jhon, M. H.; Chan, Y. Ultralow-Threshold Multiphoton-Pumped Lasing from Colloidal Nanoplatelets in Solution. *Nat. Commun.* **2015**, *6*, 8513.
(53) Yeh, S.; Wu, T.; Wei, K.; Sun, Y.; Liang, K. Effect of Incorporated CdS Nanoparticles on the Crystallinity and Morphology of Poly(styrene-b-ethylene oxide) Diblock Copolymers. *J. Polym. Sci., Part B: Polym. Phys.* **2005**, *43*, 1220−1229.
(54) Achtstein, A. W.; Ballester, A.; Movilla, J. L.; Hennig, J.; Climente, J. I.; Prudnikau, A.; Antanovich, A.; Scott, R.; Artemyev, M. V.; Planelles, J.; Woggon, U. One- and Two-Photon Absorption in CdS Nanodots and Wires: the Role of Dimensionality in the One- and Two-Photon Luminescence Excitation Spectrum. *J. Phys. Chem. C* **2015**, *119*, 1260−1267.
(55) Säynätjoki, A.; Karvonen, L.; Riikonen, J.; Kim, W.; Mehravar, S.; Norwood, R. A.; Peyghambarian, N.; Lipsanen, H.; Kieu, K. Rapid Large-Area Multiphoton Microscopy for Characterization of Graphene. *ACS Nano* **2013**, *7*, 8441−8446.
(56) Shahin, S.; Mehravar, S.; Gangopadhyay, P.; Peyghambarian, N.; Norwood, R. A.; Kieu, K. Multiphoton Microscopy as A Detection Tool for Photobleaching of EO Materials. *Opt. Express* **2014**, *22*, 30955−30962.
(57) Thienpont, H.; Rikken, G.; Meijer, E.; Ten Hoeve, W.; Wynberg, H. Saturation of the Hyperpolarizability of Oligothiophenes. *Phys. Rev. Lett.* **1990**, *65*, 2141.
(58) Dong, A.; Ye, X.; Chen, J.; Kang, Y.; Gordon, T.; Kikkawa, J. M.; Murray, C. B. A Generalized Ligand-Exchange Strategy Enabling Sequential Surface Functionalization of Colloidal Nanocrystals. *J. Am. Chem. Soc.* **2011**, *133*, 998−1006.
(59) Rosen, E. L.; Buonsanti, R.; Llordes, A.; Sawvel, A. M.; Milliron, D. J.; Helms, B. A. Exceptionally Mild Reactive Stripping of Native Ligands from Nanocrystal Surfaces by Using Meerwein's Salt. *Angew. Chem., Int. Ed.* **2012**, *51*, 684−689.

DOI: 10.1021/acs.macromol.6b00926
Macromolecules 2016, 49, 5068−5075